KSCE Journal of Civil Engineering (2023) 27(12):5268-5280
DOI 10.1007/s12205-023-2174-6

pISSN 1226-7988, eISSN 1976-3808
www.springer.com/12205

Structural Engineering

Flexural Strengthening of Two-Way RC Slabs with Textile Reinforced Mortar: Experimental Study and Calculation Model

Zongcai Deng[a], **Qian Xia**[b], **Minggao Gong**[a], **and Junlin Xu**[a]

[a]*Key Laboratory of Urban Security and Disaster Engineering, Ministry of Education, Beijing University of Technology, Beijing 100124, China*
[b]*Jingyeda New Building Materials Co. Ltd., Beijing 100124, China*

ARTICLE HISTORY

Received 17 November 2022
Revised 28 May 2023
Accepted 21 August 2023
Published Online 28 October 2023

KEYWORDS

Textile reinforced mortar
Two-way slab
Flexural capacity
The theory of plastic hinges
Fiber strength utilization rate
Shear capacity

ABSTRACT

Textile reinforced mortar (TRM) strengthening can improve the anti-aging performance of reinforced concrete (RC) slabs, and significantly improve the rust problem of steel plates and bending performance of RC slabs. To study the effect of TRM on the flexural capacity of two-way RC slab, four sided simply supported bending tests were conducted on two TRM strengthened concrete slabs and an unstrengthened control slab. And the effects of different strengthening techniques on the flexural capacity and bending deformation capacity of the two-way RC slabs were investigated. It was concluded that the application of TRM to strengthen the two-way RC slabs can effectively improve its bending bearing capacity and bending deformation capacity. Compared with the unstrengthened control slab, the bending bearing capacity of the two strengthened slabs increased by 54.2% and 43.8%, respectively, and the energy absorption value increased by 75.5% and 49.1%, respectively. In addition, compared with control slab, the post-cracking stiffness of TRM reinforced slabs treated with and without interface agents increased by 145.2% and 83.4%, respectively. This indicated that using interface agents for interface treatment could improve the adhesion between the TRM and the original RC slab, thereby preventing the initiation and development of cracks between the new and old interfaces. The strength utilization rate of textile was proposed, and the relationship between strength utilization rate of textile and maximum or minimum distribution network rate was analyzed. Based on the plastic hinge theory a simple calculation formula for the bending bearing capacity of the two-way RC slab strengthened with TRM was proposed, which provided the reference for the application of TRM for strengthening projects.

1. Introduction

Traditional reinforced concrete structures have been widely used in various structural components with the characteristics of high compressive strength, good durability and low price. Various concrete structural components have gradually exposed problems such as steel corrosion and cracks during the service of structures (Scheerer et al., 2015). Meanwhile, the bearing capacity of structural components was insufficient due to material aging and environmental erosion. Problems such as the decrease in stiffness have attracted the attention of experts and scholars, and the research on the retrofitting of traditional RC structures is urgent.

Fiber reinforced polymer mortar (FRPM) has been widely used in engineering strengthening with the characteristics of light weight, high strength, excellent durability and corrosion resistance, and convenient construction. However, some drawbacks have been observed during the use of FRPMs because of the epoxy resins. These drawbacks include poor high temperature and fire resistance, poor construction performance in low temperature and humid environments because of poor moisture permeability (Al-Salloum et al., 2011).

To solve these difficulties, a new type of fiber reinforced cementitious composite, textile reinforced mortar (TRM), also known as textile reinforced concrete (TRC), had been suggested for structural strengthening (Triantafillou and Papanicolaou, 2006). TRM is a composite embedding multiaxial textile made of carbon, basalt or glass into inorganic materials such as cement-based mortars. With good durability and corrosion resistance, the

CORRESPONDENCE Zongcai Deng dengzc@bjut.edu.cn Key Laboratory of Urban Security and Disaster Engineering, Ministry of Education, Beijing University of Technology, Beijing 100124, China

required protective layer of TRM is small, which enables it to strengthen the structures without changing the cross-sectional size of the components, and effectively reduce the weight of the structures (Scheerer et al., 2019). In addition, it has a good compatibility deformation with the original structure. Compared to FRPMs, TRM can achieve better performance in humid and corrosive environment.

In recent years, a significant number of studies have been focused on the exploitation of TRM in retrofitting RC structural members, such as confinement of RC columns (Thermou et al., 2019), shear retrofitting of RC elements (Azam and Soudki, 2014), flexural strengthening of one-way (Schladitz et al., 2012) and two-way RC slabs (Schladitz et al., 2012) studied the flexural performance of a large-span one-way slab strengthened with carbon fiber net (CFN) with a thickness of 0.23 m and an effective span of 6.75 m through the four-point loading test method. The results showed that compared to the unstrengthening slab, slabs strengthened with TRM had a great improvement in bearing capacity and smaller deflection and finer cracks under the same load, indicating that TRM can be used to strengthen the large-span structural members (Papanicolaou et al., 2009) conducted related experimental studies on the two-way RC slabs strengthened with TRM, and the results showed that CFN can effectively improve the load-bearing and energy dissipation capacity of the two-way RC slabs, and the increase in bearing capacity was proportional to the number of TRM layers (one layer 26%, two layers 53%) (Koutas and Bournas, 2017) conducted an experimental study on the flexural performance of five two-way RC slabs strengthened with TRM. The results showed that with the increase of the TRM layers, the stiffness and cracking load of the slab were effectively improved. The application of local strengthening can effectively improve the utilization rate of the fiber net. Based on the test results, the theoretical flexural capacity of the TRM two-way slab was derived. However, previous studies on two-way RC slabs strengthened with TRM mostly failed in punching shear without developing a plastic failure. Investigated the flexural performance and energy dissipation capacity of basalt fiber net, alkali-resistant glass fiber net, and steel wire net strengthened normal concrete two-way slabs and ultra-high performance concrete two-way slabs. The results showed that increasing the number of layers of fiber net could effectively improve the bearing capacity, deformation energy, and energy dissipation capacity of the slab, and the reinforcement effect of alkali resistant glass fiber net was better than that of basalt fiber net, reducing the net holes spacing was beneficial for improving the bearing capacity and bending toughness of the beam (Deng and Gong, 2022; Deng et al., 2022).

Most of the studies have focused on the uniaxial strengthening performance of TRC or TRM, the exploitation of TRM for increasing the flexural capacity of two-way RC slab has rarely investigated up to now. And there are few experimental studies on the application of different interface treatments when using TRM to strengthen the two-way RC slab.

Therefore, in this paper, different interface treatment methods were adopted to deal with the interface of the two-way RC slab. For this aim, three two-way RC slabs were experimentally tested by a four-point monotonic loading method. And a calculation model for the flexural capacity of the TRM-strengthened two-way RC slab was proposed based on the results.

In previous studies, there were few studies on the bending bearing capacity of RC two-way slab using carbon fiber net. This article provided experimental data on the flexural bearing capacity of strengthened RC two-way slabs using carbon fiber net through experimental research. The use of epoxy interface agent at the interface between TRM and concrete had improved the bonding strength between the reinforcement layer and the original concrete slabs, effectively preventing local debonding failure of the strengthened layer, and improving the bending performance and load-bearing capacity of the component. The method of reinforcing concrete two-way slabs with CFN overcome the problem of steel plates being prone to rusting in steel plate reinforcement, and solved the problems of aging of polymer adhesives strengthened with carbon fiber sheets. It solved the problems of easy debonding of polymer reinforced with fiber sheets. It also solved the problem of poor fire resistance in FRPM reinforcement and improved the fire resistance of components.

2. Experimental Program

2.1 Specimens and Parameters

A total of 3 two-way RC slabs were designed in this experiment. As shown in Fig. 1, the slabs had a length of 1,800 mm and a width of 1,300 mm (rectangular slabs), and it had a thickness of 80 mm, whereas the effective span in the two directions were 1,600 mm and 1,100 mm, as shown in Fig. 2.

All slabs were lightly reinforced with ribbed steel bars to simulate the slabs to be strengthened. The ribbed steel bars whose diameter was 8 mm were placed at the bottom of the midspan in a space of 150 mm and 200 mm in the long and wide directions (Fig. 3). The role of different interface treatment methods between the slab and the strengthening layer was investigated. A specific strengthening plan was descripted Table 1.

Among them, the slab PC was tested without strengthening.

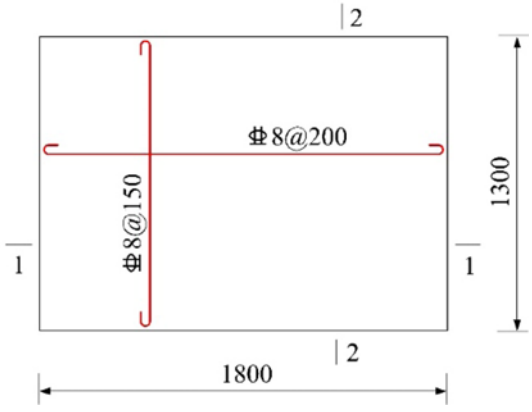

Fig. 1. The Section View of Reinforcement of Slab (unit: mm)

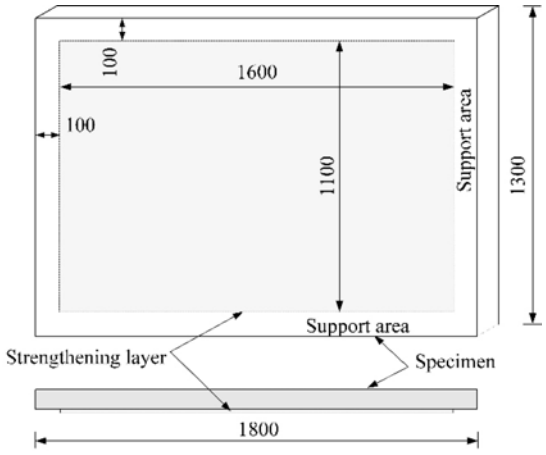

Fig. 2. Schematic Diagram of Strengthening Layer (unit: mm)

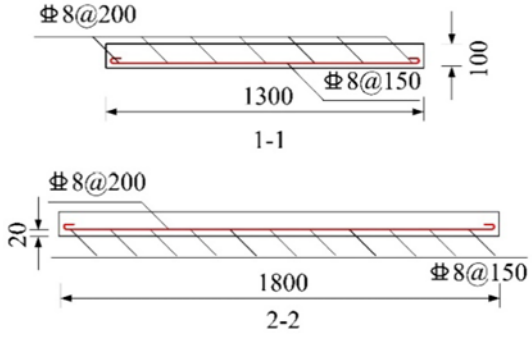

Fig. 3. The Size and Reinforcement of Slab (unit: mm)

Table 1. Specimen Code and Strengthening Plan

Specimen	Strengthening plan
PC	Control specimen
C2-epoxy	Two layers of CFN strengthening with epoxy interface agent
C2	Two layers of CFN strengthening without epoxy interface agent

The slab C2 was strengthened with two layers of CFN at the bottom and the slab C2-epoxy was brushed with epoxy interface agent on this basis to enhance the bond strength between the original structure and the strengthening layer.

2.2 Materials and Strengthening Procedure

The average compressive strength tested by concrete cubes with dimensions of 100 mm × 100 mm × 100 mm was 19.0 MPa. The ribbed steel bars had a yield strength of 460.8 MPa, a tensile strength of 596.4 MPa.

The carbon fiber net (CFN) used in this experiment, was composed of carbon fiber yarns in both warp and weft directions with a net center spacing of 20 mm, as shown in Fig. 4. The mechanical properties of CFN were shown in Table 2.

There were 2 strands of 12 K continuous carbon fiber rovings in the warp direction and 1 strand of 24 K continuous carbon fiber rovings in the weft direction. This two directions of fiber rovings were woven or knitted horizontally with the fiber rovings in the weft direction passing through 2 fiber rovings in the warp direction at the orthogonal points. Then this fiber rovings were fixed by hot melt glue lines, and the surface was covered and heated to solidify.

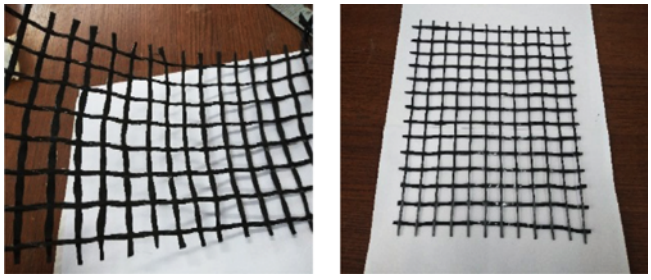

Fig. 4. Carbon Fiber Net

Table 2. Performance Parameters of CFN

Tensile strength (MPa)	Elastic modulus (GPa)	Ultimate load of single yarn (N)	Theoretical thickness (mm)	Areal density (g/m^2)
2,300	230	3,200	0.044	80

Table 3. Parameters of Special Mortar for CWSM Carbon Fiber Net

Splitting tensile strength (MPa)	Flexural strength (MPa)	Tensile bond strength (MPa)	Compressive strength (7d/28d) (MPa)	Bonding strength with CFN (kN/m)
7	12	2.5	40/55	200

In this experiment, a special fiber reinforced polymer mortar (FRPM) was applied as the bonding material. There were a large number of advantages using FRPM including good fire resistance, excellent air permeability, no shrinkage and strong adhesion. It can not only ensure the bond strength with the original structure, but also had better grip strength with CFN. The performance parameters of FRPM were shown in Table 3. When mixing FRPM, added 2.5 kg/m^3 polyvinyl alcohol (PVA) fiber, whose length and diameter were 6 mm and 28.3 μm, respectively. The tensile strength and the modulus of elasticity of PVA were 1,280 MPa and 26.8 GPa, respectively.

The process of strengthening was as follows (Fig. 5): 1) Remove the floating ash of the surface, and chisel the base surface; 2) Apply a layer of epoxy interface agent on the base surface of the slab C2-epoxy whose performance parameters are shown in Table 4; 3) Mix the FRPM and apply the first layer of 5 mm thick FRPM before the interface agent was dry; 4) Lay the first layer of CFN with a lap length of 20 mm, and ensure that the CFN was laid flat; 5) Spread 2 – 3 mm thick FRPM mortar on the surface of the first layer of CFN and lay the second layer of CFN; 6) After the first layer of FRPM was initially harden, apply the second layer of FRPM with a thickness of 7 – 8 mm, and control the total thickness of CFN and FRPM to 15 mm; 7) Spray water to maintain FRPM to age.

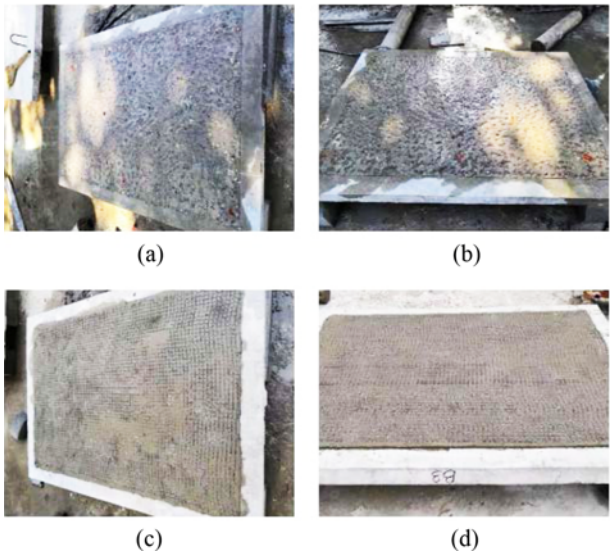

Fig. 5. TRM Strengthening Application Steps: (a) Concrete Surface Preparation, (b) Dampening of Surface and Brush Interface Agent to Receive Strengthening, (c) First Mortar and CFN Layer Application, (d) Final Finished Surface

Table 4. Performance Parameters of Epoxy Interface Agent

Tensile strength (MPa)	Flexural strength (MPa)	Compressive strength (MPa)	Tensile shear strength (MPa)
45	130	94	16

2.3 Test Setup and Procedure

To simulate the uniform load in the actual project, a four-point loading method was adopted in the test. The specific force transmission route was the reaction frame, the actuator, the distribution beam, and the rigid distribution iron, as shown in Fig. 6. The loading process was divided into pre-loading and final loading. The purpose of pre-loading was to check whether each part of the device was in good contact and whether the strain gauges and displacement gauges worked normally. A graded loading method was adopted in the final loading. Before the slab cracked, the load was increased by 5 kN per level, when the slab was close to cracking, the load was increased by 2 kN per level until the slab cracked; After the slab yielded, the load was increased by 2 kN per level until it failed. Each level of load lasted for 2 minutes. Observing and recording the failure mode of the slab and the development of cracks during this stage.

3. Test Results and Analysis

The main test results were given in Table 5, including the ultimate load and its corresponding central deflection, the pre-cracking stiffness and the post-cracking stiffness. Among them, the pre-cracking stiffness was calculated based on the tangent stiffness of the load versus central deflection curve of the slab before it cracked, while the post-cracking stiffness was calculated based on the tangent stiffness of the load versus central deflection curve of the slab after it cracked.

3.1 Load-Deflection Curve

The load versus central deflection curves of all specimens were shown in Fig. 7. All curves in Fig. 7 were divided into three distinct stages: 1) Uncracked stage: It had an approximate linear elastic relationship between load and deflection, and this stage ended as the concrete cracked; 2) Yield stage: Both steel and

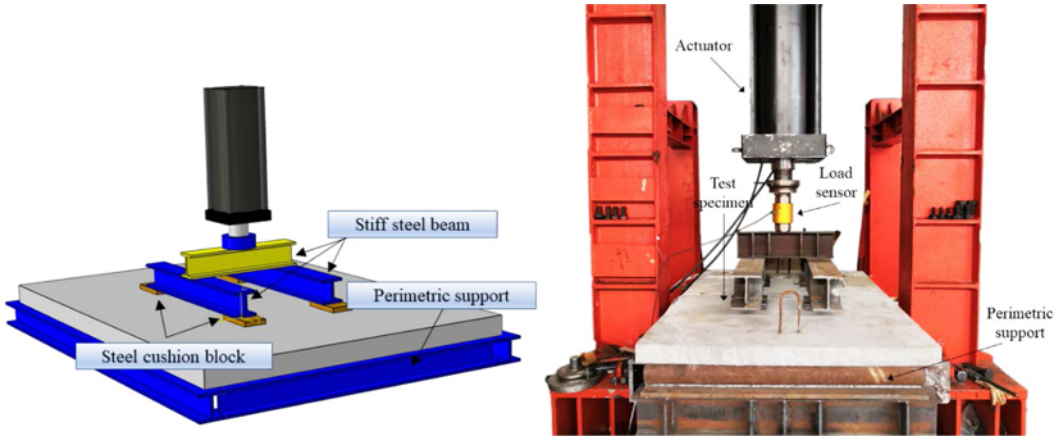

Fig. 6. Test Setup

Table 5. Summary of Main Test Results

Specimen	Peak load P_{max} (kN)	Midspan deflection at P_{max} (mm)	Capacity increase (%)	Pre-cracking stiffness (kN/mm)	Post-cracking stiffness (kN/mm)
PC	150.43	51	—	16.5(100%)	1.57(100%)
C2-epoxy	231.94	23	54.2	24.4(147.8%)	3.85(245.2%)
C2	216.28	35	43.8	20.5(124.2%)	2.88(183.4%)

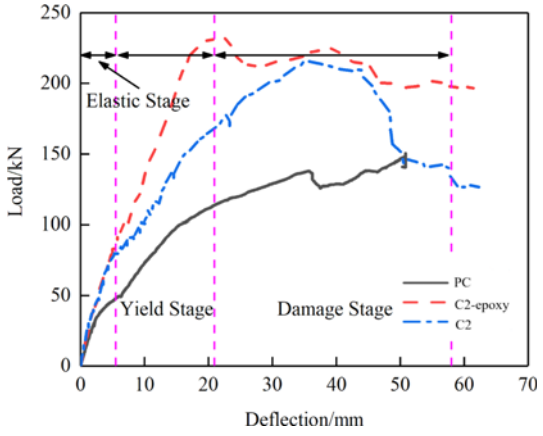

Fig. 7. Load Versus Central Deflection Curves

TRM strengthening were fully activated in tension so as to increase the flexural capacity during this stage, and the cracks developed rapidly until the tensile reinforcement at the bottom of the slab yielded; 3) Failure stage: Slab PC entered plastic stage in this stage; While for strengthened ones, the contribution of the steel reinforcement remained almost unchanged, and the increase of flexural resistance in this stage substantially attributed to further activation of TRM. It can be seen from Fig. 7 and Table 5 that compared to the slab PC, the bearing capacity and stiffness of the strengthened slabs were significantly increased.

3.2 Failure Modes and Ultimate Load

The failure modes and crack patterns of all specimens were shown in Fig. 8. The failure modes of the strengthened slab were that the crush of the concrete followed by the tensile reinforcement yielded, indicating it was under-reinforced. The cracking load, yield load and ultimate load of the slab PC were 34 kN, 100 kN and 150 kN, respectively, and the corresponding central deflection were 2.54 mm, 15.49 mm and 50.85 mm, respectively. It can be seen from Fig. 8 that when the slab PC failed, the deflection was large and the crack at the bottom of the slab was wide. Before the slab cracked, the load and the central deflection showed an approximate linear relationship. When the load increased to 34 kN, the first orthogonal bending crack appeared in the loading area of the slab along the longitudinal reinforcement direction. The central cracks at the bottom of the slab gradually expanded to the corners and surroundings with the load continued to increasing. The reinforcement at the tensile area of the slab yielded when the load increased to 100 kN. As approaching the ultimate load, the diagonal cracks (J1, J2, J3, J4) in the corner area expended to the edge of the slab, forming a typical plastic hinge line pattern.

All strengthened slabs failed due to the loss of strengthening effect. There were two failure modes in the strengthened slabs:

1. In the central largest bending moment area, the cracks were too wide to cause the CFN to be partially broken and slipped in the mortar. The final cracks were too large to bear the applied load (slab C2). This type of failure mode was common in C-TRM strengthening materials in the experimental research of C-FRCM strengthened RC beams reported in the literature (D'Ambrisi et al., 2012). In the process of fiber slippage, the bridge effect of the fibers gradually decreased, and finally the residual bearing capacity of the specimens was roughly the same as that of the control slab. This can be confirmed by the downward trend of the load versus central deflection curve. Observing the cracks at the bottom of the slab from a macro perspective, the broken fibers here were not obvious.
2. Delamination or interlaminar shear at the matrix fabric interface. In this case, the shear strength between the TRM matrix and the concrete was greater than the shear strength between the TRM matrix and the CFN (Loreto et al., 2013). From the load versus central deflection curve, it showed that the residual bearing capacity of slab did not change much, but its central deflection continued to increase.

The failure process of the strengthened slabs was roughly the same. In the linear elastic stage, the load had an approximate linear relationship with the central deflection. The positive bending moment at the bottom of the slab was mainly borne by the reinforcement, and the strengthening layer played a small role. When the slope of the load versus central deflection curve changed, orthogonal bending cracks (Z1, Z2, Z3, Z4) appeared in the center of the slab close to the loading area. The cracking load of the slab C2 was 99 kN, higher than the 79 kN of slab C2-epoxy, which was much higher than the cracking load of the slab PC. This was because the CFN in the strengthening layer was activated to some extent after the concrete in the tensile area cracked (Koutas et al., 2019); In the yield stage, the number of cracks continued to increase and expand outward after cracked. The load was gradually transferred from the reinforcement to the strengthening layer thus CFN started to be tensioned, and the

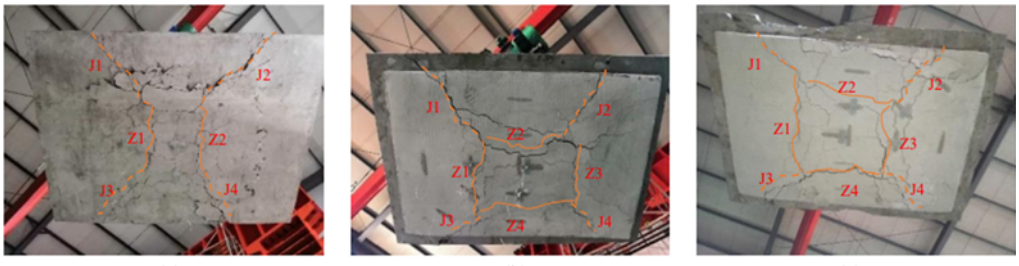

Fig. 8. Crack Pattern at the bottom Face of Tested Specimens: (a) B1, (b) B2, (c) B3

internal force redistribution process occurred between them. The stiffness of the slab at this stage was greater than the PC slab. When the reinforcement yielded, the contribution of the TRM to the flexural bearing capacity become significant, and the increasing load after the yield point was almost all borne by the strengthening layer. In the failure stage, it can be seen from Fig. 8 that the load of the slab C2-epoxy did not change much but the deflection continued to increase until the main crack was too large to bear the load. After reaching the peak load, the load versus central deflection curve of the slab C2 showed a stepwise downward trend. The fiber net continued to be broken during the process, and then the slab was damaged due to the load falling to a low point. The cracks at the bottom of the strengthened slab were similar in shape, and the plastic hinge line pattern was in an "inverted cone" shape, which was related to the loading area. It can be seen from the failure process and shape of each tested slab that the CFN strengthening system can effectively limit the deformation of the RC slab and enhance the bending resistance. The TRM reinforcement layer of the C2 slab and the local area of the new and old concretes initiated small cracks. As the load increased, the micro cracks gradually expanded along the section direction, but the extension length was limited. Due to the good overall bonding between the reinforcement layer and the original concrete, there was no significant slip between the TRM reinforcement layer and the concrete. However, no cracks were observed at the interface between the TRM reinforcement layer and concrete of the C2-epoxy slab due to the application of epoxy interfacial agent. Compared to C2 slab, C2-epoxy slab had a higher load-bearing capacity, and the load center deflection curve decreases more slowly after reaching its peak. Which indicated that the epoxy-based interface agent can achieve the strong adhesion and common force between the FRPM and the concrete interface.

It can be seen from Fig. 8 and Table 4 that compared to the slab PC, the bearing capacity and stiffness of the specimens strengthened with TRM were significantly improved. The ultimate load of slab C2 and slab C2-epoxy increased by 43.8% and 54.2%, respectively, indicating that brushing the base surface of the RC slab with epoxy-based interface agent can better exert the performance of the CFN strengthening system. In terms of the pre-cracking stiffness, the strengthened slabs (slab C2 and slab C2-epoxy) increased by 47.8% and 24.2% compared to the slab PC. In addition, the post-cracking stiffness increased by 145.2% and 83.4%, respectively. It can be concluded that the use of TRM strengthening technique have a greater impact on the post-cracking stiffness of the RC slab.

3.3 Bearing Capacity and Stiffness Analysis

From Fig. 8 and Table 4, it can be seen that compared with PC, the pre-cracking stiffness of C2-epoxy and C2 increased by 47.8% and 24.2%, respectively, and the post-cracking stiffness increased by 145.2% and 83.4%, respectively. This indicated that TRM reinforcement can significantly improve the stiffness of the slabs. This is due to the reinforcement of a 15 mm TRM layer in the tensile zone of the RC slab, which forms a whole with the original RC slab, and the pre-cracking stiffness will inevitably increase.

Compared with the PC, the ultimate load of C2-epoxy and C2 increased by 54.2% and 43.8%, respectively, indicating that using TRM reinforcement can significantly improve the flexural bearing capacity of the slab. This is due to the high tensile strength of CFN in TRM, as well as the strong grip between mortar and CFN. When used to strengthen RC slabs, the combined force in the tensile zone can be significantly improved, thereby improving the flexural bearing capacity of the slab.

Compared with C2, the pre-cracking stiffness, post-cracking stiffness, and load-bearing capacity of C2-epoxy have increased by 23.6%, 61.8%, and 10.4%, respectively. This indicated that applying epoxy based interface agent on the base surface of RC slab can better utilize the load-bearing performance of CFN reinforcement system. There are two reasons: firstly, due to the inherent tensile and bending strength of the epoxy interface agent, its use in strengthening RC slabs can improve its performance to a certain extent; Secondly, the epoxy interface agent can increase the bonding strength between TRM and RC slabs, resulting in better overall integrity and greater stiffness, allowing TRM to be more fully utilized, and improving the bending performance of the slab.

3.4 Energy Absorption Value

The energy absorption value is a characteristic value that characterizes the deformability of the slab after cracking, which is expressed by the area enclosed by the load versus deflection curve at a specific deflection (Ebead, 2015). The calculation equation was as follows:

$$W = \int_0^{\delta} F(x)dx \,, \tag{1}$$

where W was the energy absorption value (J) of the test slab; d was the central deflection of the slab; $F(x)$ was the load value

Table 6. Energy Absorption Value of Slabs

Specimen	Energy absorption W (J)				
	δ = 10 mm	δ = 20 mm	δ = 30 mm	δ = 40 mm	δ = 50 mm
PC	387.4(100%)	1342.8(100%)	2603.6(100%)	3913.7(100%)	5406.8(100%)
C2-epoxy	657.5(169%)	2374.2(177%)	4707.5(181%)	6966.9(178%)	9313.7(172%)
C2	573.1(148%)	1934.2(144%)	3660.0(141%)	6345.9(164%)	8034.7(149%)

(kN) corresponding to the deflection.

Using the method of numerical integration to calculate the energy absorption value of the slabs under different deflection. The results were shown in Table 6.

Combining Fig. 7 and Table 6, it can be seen that compared to the slab PC, the energy absorption values of the strengthening slabs (slab C2 and slab C2-epoxy) improved 49.1% and 75.5% on average, respectively. Both two strengthening methods can effectively improve the energy dissipation capacity of the RC slab, but the latter it was more effective. That was because the epoxy-based interface agent can strengthen the effective bond of CFN strengthening system, which could give full play to the strengthening effect of CFN. However, the CFN strengthening system will debond from the matrix after the concrete cracked without interface agent, resulting in slippage and energy dissipation. As the load increased, the fiber nets were stretched and broken, and energy consumption capacity of the slab can't be fully improved.

4. Analytical Model

The analytical model was proposed based on the following assumptions:

1. Section strains conforms to the hypothesis for plane cross section;
2. Ignore tensile strength of the concrete and FRPM;
3. When the slab reached the limit state, it was divided into several rigid plates by several plastic hinge lines, and the plates meet the deformation coordination conditions;
4. After the plastic hinge line formed, the ultimate bending moment of the yield section remained unchanged;
5. Assuming that there is no relative slip between concrete and steel reinforcement, and without considering the hardening of steel reinforcement.

4.1 Material Constitutive Model

The stress-strain relationship of concrete does not consider the tensile strength of concrete. The model suggested by Rüsch (1960) is adopted. The ascending branch was a quadratic parabola, and the descending branch was a horizontal line section. The mathematical expression was

$$\sigma_c(\varepsilon_c)=\begin{cases} f_c\left(\dfrac{2\varepsilon_c}{\varepsilon_{c0}}-\left(\dfrac{\varepsilon_c}{\varepsilon_{c0}}\right)^2\right) & 0\le\varepsilon_c\le\varepsilon_{c0} \\ f_c & \varepsilon_{c0}\le\varepsilon_c\le\varepsilon_{cu} \end{cases}, \tag{2}$$

where f_c was the axial compressive strength of concrete; ε_{c0} was the compressive strain of concrete when the compressive stress of concrete reaches f_c, taken as 0.002; and ε_{cu} was the ultimate compressive strain of concrete, taken as 0.0033.

The stress-strain relationship of the steel bar adopts a completely elastic-plastic double-line model, and its mathematical expression was

$$\begin{cases} \sigma_s=E_s\varepsilon_s & 0\le\varepsilon_s\le\varepsilon_y \\ \sigma_s=f_y & \varepsilon_y\le\varepsilon_s\le\varepsilon_{su} \end{cases}, \tag{3}$$

where E_s was the elastic modulus of the steel bar; ε_f was the yield strain of the steel bar; and f_y was the yield strength of the steel bar.

CFN was a brittle material that maintains a linear elastic state before fracture. Using the linear elastic model proposed, its mathematical expression was

$$\sigma_f=E_f\varepsilon_{fe}\quad 0\le\varepsilon_{fe}\le\varepsilon_f, \tag{4}$$

where E_f was the elastic modulus of CFN; ε_{fe} was the effective strain of CFN; ε_f was the ultimate tensile strain of CFN.

4.2 Effective Stress of Fiber

Because the bending moment of each section under load was different, so the effective stress of CFN in the TRM strengthening layer when bearing the load was different from that of CFN borne load alone. When some yarns in the mid-span section reached the ultimate tensile strain and broken, while that of other sections have not reached their ultimate tensile strain. Therefore, the actual stress of CFN in FRPM was calculated by the product of its effective strain and its elastic modulus, that is

$$f_{te}=E_f\varepsilon_{fe}, \tag{5}$$

where E_f was the elastic modulus of CFN; and ε_{fe} was the effective tensile strain of CFN.

In this paper, concrete was crushed after the steel bars yielded, but the fiber net did not reach its ultimate tensile strain. According to hypothesis for plane cross sections, the strain coordination relationship among the compressive strain in the concrete, the steel tensile yield strain and the effective tensile strain of CFN was as follows:

$$\frac{\varepsilon_{cn}}{x_n}=\frac{\varepsilon_y}{d-x_n}=\frac{\varepsilon_{fe}}{H-x_n}. \tag{6}$$

The depth of the neutral axis and the effective tensile strain of CFN can be obtained as

$$x_n=\frac{\varepsilon_{cu}}{\varepsilon_{cu}+\varepsilon_y}\cdot d, \tag{7}$$

$$\varepsilon_{fe}=\frac{H-x_n}{x_n}\cdot\varepsilon_{cu}. \tag{8}$$

When the yarns were partially broken and the concrete was not crushed, the strain coordination relationship was expressed as Eq. (9)

$$\frac{\varepsilon_c}{x_n}=\frac{\varepsilon_s}{d-x_n}=\frac{\varepsilon_{fe}}{H-x_n}. \tag{9}$$

This type of failure mode was mentioned in the literature (Koutas and Bournas, 2017). Using its experimental data, referring to the

theoretical calculation method of beam (Babaeidarabad et al., 2014) strengthened by C-FRCM, the iterative method was used to calculate the depth of the neutral axis and the effective strain of fiber net, and the process was as follows:

Assuming the depth of the neutral axis as x_n, substituting the assumed value into Eq. (9), the steel tensile strain ε_s and the effective tensile strain of fiber net ε_{fe} were solved respectively. Then the strains were substituted into Eqs. (3) and (9) to calculate their stress. Finally, the depth of the neutral axis was calculated by Eq. (10) again.

$$x_n^{cal} = \frac{A_s\sigma_s + A_f E_f \varepsilon_{fe}}{\alpha_1 f_c b \beta_1}, \tag{10}$$

where α_1 and b_1 were the coefficients of the concrete rectangular stress figure, which were given by the following Eqs. (11) and (12)

$$\beta_1 = \frac{4\varepsilon_c' - \varepsilon_c}{6\varepsilon_c' - 2\varepsilon_c}, \tag{11}$$

$$\alpha_1 = \frac{3\varepsilon_c'\varepsilon_c - \varepsilon_c^{\,2}}{3\beta_1\varepsilon_c'^2}, \tag{12}$$

where ε_c' was the unconfined concrete compressive strain

$$\varepsilon_c' = 1.7 f_c / E_c, \tag{13}$$

where E_c was the concrete elastic modulus, calculated by Eq. (14)

$$E_c = 4700\sqrt{f_c}. \tag{14}$$

When the error did not exceed 1% of the calculated value, the assumption was considered valid, that is

$$\Delta = \frac{x_n - x_n^{cal}}{x_n} \le 0.01. \tag{15}$$

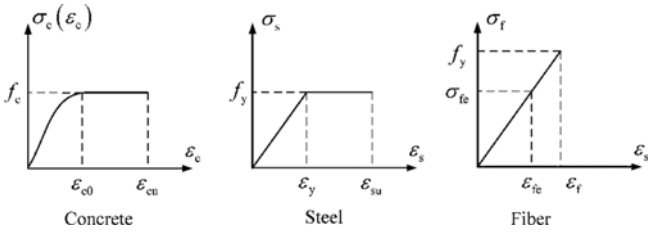

Fig. 9. Material Constitutive Model

4.3 Fiber Strength Utilization Rate

According to the derivation in Section 4.2, the effective strain of CFN was less than its ultimate tensile strain, that is $\varepsilon_{fe} \le \varepsilon_f$, the ratio of effective strain ε_{fe} to ultimate tensile strain ε_f was defined as the strength utilization rate of the fiber net, namely

$$\lambda = \frac{\varepsilon_{fe}}{\varepsilon_f} \times 100\%. \tag{16}$$

The calculation results were shown in Table 7. It can be seen that the distribution network rate was negatively correlated with the utilization rate. The power function fitting of the test data was shown in Fig. 10.

$$\lambda = 4.16\rho_f^{-0.264} \tag{17}$$

According to the Eqs. (6) to (15) in section 4.2, the parameter values of each specimen were calculated and summarized in Table 7.

4.4 Analysis of Critical Failure State

When the two-way slab strengthened by TRM reached the failure state, it may be that the concrete in the compression zone was crushed or the fiber net in the reinforcement layer was broken or slipping. In this case, the following three critical failure states were obtained.

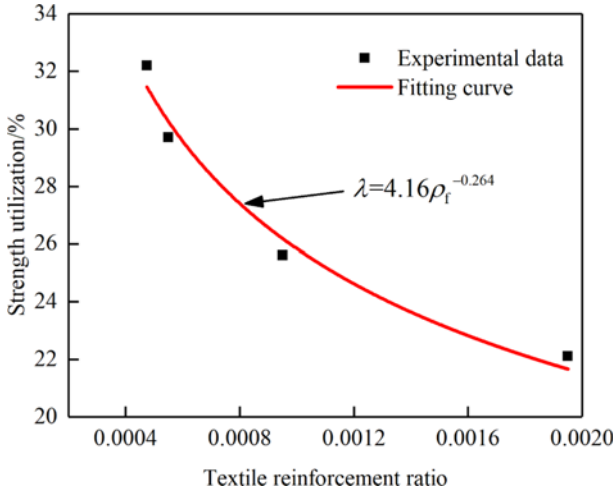

Fig. 10. Power Function Fitting Curve of Strength Utilization and Textile Reinforcement Ratio

Table 7. Summary of Parameters of Tested Slabs

Data sources	Specimen	ε_c	ε_c'	x_n		α_1	β_1	ε_{fe}		l
				x	y			x	y	
This paper	PC	0.0033	0.00158	10.36	7.76	1.000	0.800	—	—	—
	C2-epoxy	0.0033	0.00158	33.00	28.29	1.000	0.800	4.70×10^{-3}	6.03×10^{-3}	29.7
Koutas and Bournas (2017)	C1	0.00095	0.00161	18.25		0.707	0.670	4.33×10^{-3}		25.6
	C2	0.0011	0.00161	22.75		0.715	0.738	3.74×10^{-3}		22.1
	C1-part	0.00095	0.00189	14.88		0.700	0.598	5.43×10^{-3}		32.2
	G3	0.00075	0.00189	15.63		0.692	0.498	4.05×10^{-3}		—

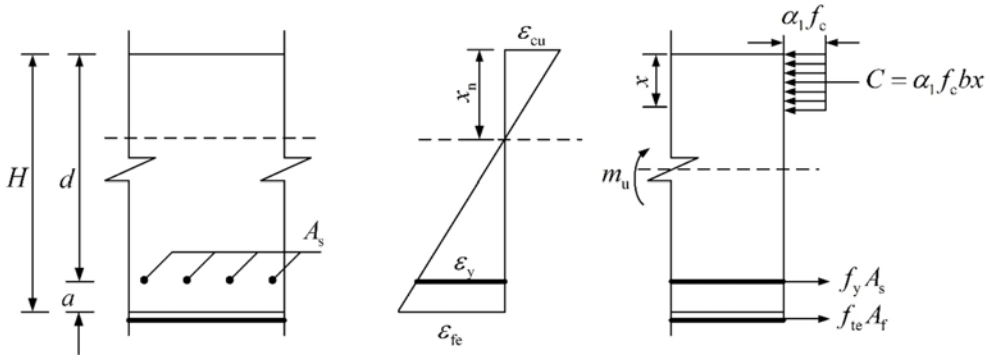

Fig. 11. State I Section Strain Relation and Stress Diagram

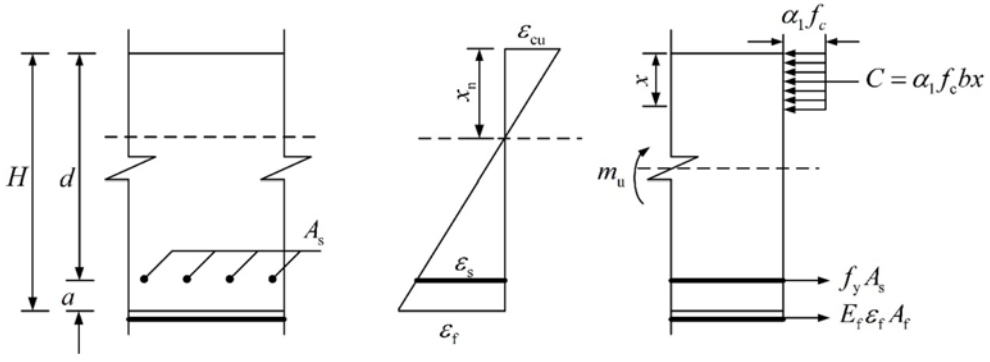

Fig. 12. State II Section Strain Relation and Stress Diagram

4.4.1 Failure State I

The concrete crushed and the reinforcement yielded when the slab failed, but the strain of the CFN did not reach the ultimate tensile strain, that is, $\varepsilon_c = \varepsilon_{cu}$, $\varepsilon_s = \varepsilon_y$. At this time, the depth of the neutral axis was

$$x_{nb1} = \frac{\varepsilon_{cu}}{\varepsilon_{cu} + \varepsilon_y} \times d \ . \tag{18}$$

The schematic diagram of the section force was shown in Fig. 11. The force balance relationship was showed as Eqs. (19) and (20)

$$f_c b \beta_1 x_n = A_s f_y + A_s f_{te} \ , \tag{19}$$

$$m_u = A_s f_y \left(d - \beta_1 x_n / 2\right) + A_s f_{te} \left(H - \beta_1 x_n / 2\right) , \tag{20}$$

where A_s is the reinforcement area per 1 m (mm^2/m); A_f is the CFN area per 1 m (mm^2/m); m_u is the ultimate flexural capacity of the slab per 1 m ($m_{u,x}$ in the x direction, and $m_{u,y}$ in the y direction); β_1 is the coefficient of the rectangular stress figure, taken as 0.8.

4.4.2 Failure State II

The concrete crushed and the CFN reached its ultimate tensile strain ε_f when the slab failed, and the depth of the neutral axis was

$$x_{nb} = \frac{\varepsilon_{cu}}{\varepsilon_{cu} + \varepsilon_f} \cdot H \ . \tag{21}$$

The schematic diagram of the section force was shown in Fig. 12. The force balance relationship was shown as Eqs. (22) and (23)

$$f_c b \beta_1 x_n = A_s f_y + A_f E_f \varepsilon_f \ , \tag{22}$$

$$m_u = A_s f_y \left(d - \beta_1 x_n / 2\right) + A_f E_f \varepsilon_f \left(H - \beta_1 x_n / 2\right) . \tag{23}$$

4.4.3 Failure State III

The concrete of the compression zone reached ε_{c0}, and the CFN reached its ultimate tensile strain ε_f when the slab failed. The depth of the neutral axis was

$$x_{nb3} = \frac{\varepsilon_{c0}}{\varepsilon_{c0} + \varepsilon_f} \cdot H \ . \tag{24}$$

The schematic diagram of the section force was shown in Fig. 13. The force balance relationship was shown as Eqs. (25) and (26)

$$C = \int_0^{x_n} \sigma_c b dy = A_s f_y + A_f E_f \varepsilon_f \ , \tag{25}$$

$$m_u = A_s f \left(d - x_n + Y\right) + A_f E_f \varepsilon_f \left(H - x_n + Y\right) , \tag{26}$$

where C was the resultant force in the compression zone; Y was the distance from the resultant force in the compression zone to the neutral axis of the section.

4.5 Maximum and Minimum Textile Ratio

To avoid material waste caused by excessive distribution network or

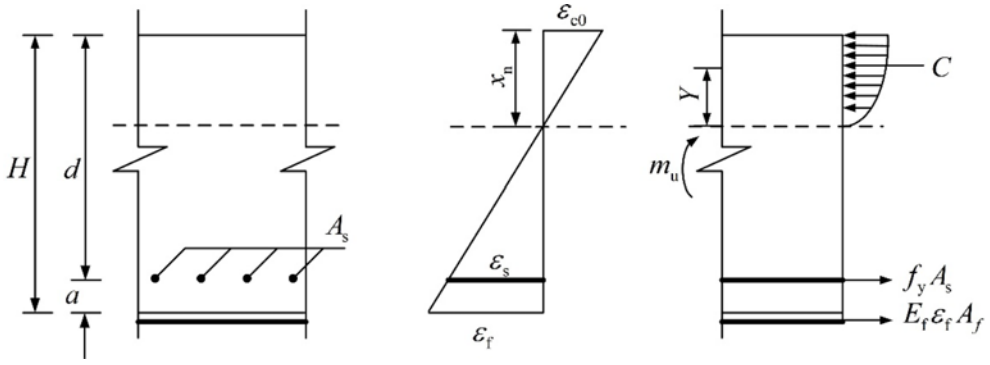

Fig. 13. State I Section Strain Relation and Stress Diagram

insufficient bearing capacity of two-way slab caused by few distribution network, the concepts of maximum distribution network ratio and minimum distribution network ratio were proposed to provide reference for strengthening design.

4.5.1 Maximum Textile Ratio

Considering the maximum and minimum reinforcement ratio of the slab without strengthening, a compression failure similar to an over-reinforced member would happen when the textile ratio was too high, resulting in material waste. Define the maximum textile ratio as when the concrete in the compression zone crushed and the tensile reinforcement yielded.

$$\rho_{t,\max} = \frac{A_{f,\max}}{bd} = \frac{f_c \xi_b - f_y \rho_s}{f_{te}}, \tag{27}$$

where $\rho_{t,\max}$ was the maximum ratio of the strengthened slab; $A_{f,\max}$ was the maximum fiber area per 1 m (per direction) (mm^2/m); b was the unit width (mm); d was the effective depth of the slab (mm); ξ_b was the relative limit height of the compression zone; f_y was the steel yield strength (MPa); ρ_s was the reinforcement ratio in a certain direction of the slab; f_{te} was the effective tensile stress of the CFN (MPa).

4.5.2 Minimum Textile Ratio

If the textile ratio is too low, the compressive strain of the concrete is small when the slab failed, which is considered to be brittle failure. Thus defining the minimum textile ratio as $\varepsilon_c = \varepsilon_{c0}$.

$$\rho_{t,\min} = \frac{A_{f,\min}}{bd} = \frac{1}{f_{te} d}\left(\frac{2 f_c H \varepsilon_{c0}}{3\left(\varepsilon_{c0} + \varepsilon_f\right)} - \frac{f_c A_s}{b}\right), \tag{28}$$

where $\rho_{t,\min}$ is the minimum textile ratio of the strengthening slab; $A_{f,\min}$ is the minimum fiber area per 1 m (per direction) (mm^2/m); H is the section height equal to the slab thickness (mm).

5. Calculation of Theoretical Bearing Capacity

5.1 Theoretical Analysis of Plate Plastic Hinge Line

According to the failure modes of the tested slabs and the crack form at the bottom of the slab, the following two plastic hinge modes were obtained. Then the theoretical bearing capacity of the strengthened slabs was calculated and compared to the test value.

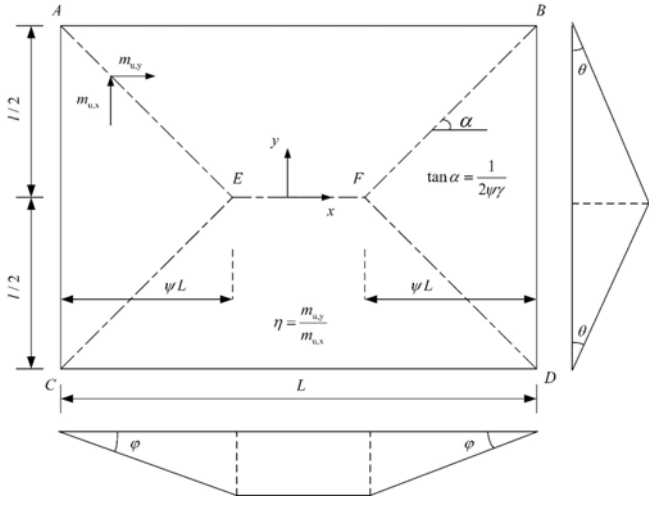

Fig. 14. Plastic Hinge Mode I

5.2 Plastic Hinge Line Mode-I

According to the specific failure mode of the tested slab in section 3.2 of this paper, it can be seen that the slab PC only had the main crack parallel to the edge of the slab in the long-span direction, and then gradually expanded to the corner as the load increasing, so it was simplified as shown in Fig. 14.

The angular displacement of each plastic hinge line was

$$\varphi = 1/\psi L, \theta = 2/l, \tag{29}$$

where φ was the angular displacement of plate ACE; θ was the angular displacement of plate ABEF; and ψ was the position parameter of the plastic hinge line (Burgess, 2017).

$$\psi = \frac{1}{2\gamma^2\eta}\left(\sqrt{3\eta\gamma^2} - 1\right). \tag{30}$$

where g was the aspect ratio of the slab, $\gamma = L/l$; h was the ratio of moments per 1 m, $\eta = m_{u,y}/m_{u,x}$.

The displacement of the loading point was

$$\omega_0 = (l-2c)/l\ , \tag{31}$$

where c was the vertical distance between the loading point and the plastic hinge line EF.

Total virtual internal work was

$$U = 2m_{u,x}L\theta + 2m_{u,y}l\varphi = 4(\gamma+\eta\tan\alpha)m_{n,x}\ . \tag{32}$$

Total virtual external work was

$$W = gV + 4P_0\omega_0 = g\left[(2\psi/3+1/2)L\cdot l - l^2/2\right] + 4P_0\omega_0\ . \tag{33}$$

From the principle of virtual work

$$P_0 = \left[(\gamma+\eta\tan\alpha)\cdot l/(l-2c)\right]m_{u,x} - G_g\ , \tag{34}$$

where P_0 was the concentrated force on the loading point when the slab failed; V was the volume enclosed by the virtual displacement of the slab; and G_g was the self-weight effect, which can be calculated by the following Eq. (35)

$$G_g = gl\left[(2\psi/3+1/2)L\cdot l - l^2/2\right]/4(l-2c)\ . \tag{35}$$

5.3 Plastic Hinge Mode Line-II

It can be seen from Fig. 8 that the slab C2-epoxy and C2 presented an "inverted cone" failure mode. The tested slab was divided into 5 rigid plates. Assuming that the middle rigid plate just surrounded the 4 loading points, the failure mode was simplified as Fig. 15.

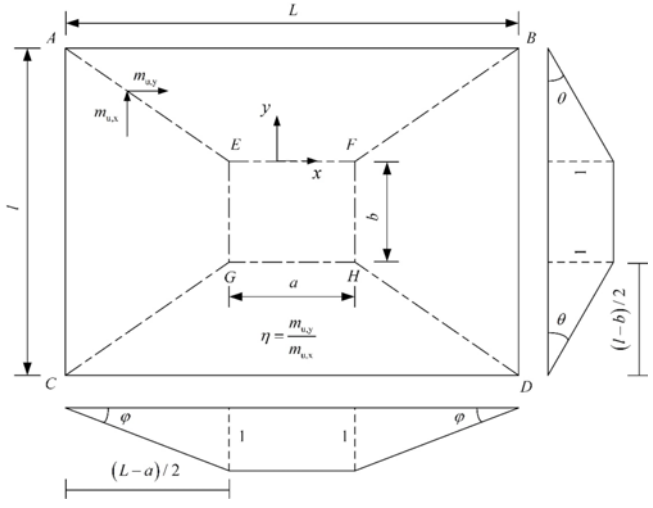

Fig. 15. Plastic Hinge Mode II

The angular displacement of each plastic hinge line was

$$\theta = 2/(l-b), \varphi = 2/(L-a)\ , \tag{36}$$

where a and b are the distances between the loading points in the x and y directions, respectively.

Total virtual internal work was

$$U = 4\left[m_{u,x}L/(l-b) + m_{u,y}l/(L-a)\right]\ . \tag{37}$$

Total virtual external work was

$$W = gV + 4P_0\omega_0 = \frac{1}{3}g\left(a\cdot b + L\cdot l + \sqrt{a\cdot b\cdot L\cdot l}\right) + 4P_0\ . \tag{38}$$

From the principle of virtual work

$$P_0 = \left(\frac{\gamma}{1-b/l} + \frac{\eta}{\gamma-a/l}\right)m_{u,x} - G_g\ , \tag{39}$$

where G_g is the self-weight effect of the slab, which can be calculated by the following Eq. (40)

$$G_g = \frac{1}{12}g\left(a\cdot b + L\cdot l + \sqrt{a\cdot b\cdot L\cdot l}\right)\ . \tag{40}$$

5.4 Comparison of Experimental Value and Theoretical Value

Table 8 showed the comparison between the theoretical bearing capacity and the experimental bearing capacity under different plastic hinge line modes. From the data in Table 8, it can be seen that under the plastic hinge line mode-I, the theoretical bearing capacity of the slab B2 was 194 kN. The ratio to the experimental bearing capacity was 0.90; The value under the plastic hinge line mode two was 210 kN, and the ratio to the experimental bearing capacity was 0.97. It can be seen that the theoretical bearing capacity under the plastic hinge line mode two was closer to the actual bearing capacity of the test, indicating that the second failure mode was closer to the actual failure mode of slab C2-epoxy, which was also correspond the actual failure mode of the tested slab. When calculating the bearing capacity of the slab PC using the Eqs. (29) to (35) and Eqs. (36) to (40), the ratios of the theoretical calculation bearing capacity to the actual experimental bearing capacity in mode one and mode two were 0.69 and 0.81, respectively, which were both conservative because of the membrane effect after the reinforcement yielded. It was believed that the slab would lose the bearing capacity when the CFN was

Table 8. Experimental and Theoretical Values of Capacity

Data sources	Specimen	ρ_f / %	f_{te} (MPa)		$m_{u,theory}$		P_{exp}	P_{theory}		P_{theory}/P_{exp}	
			x	y	x	y		I	II	I	II
This paper	PC	—	—	—	8.02	5.22	150	103	121	0.69	0.81
	C2-epoxy	0.055	1,081	1,388	12.96	12.63	216	194	210	0.90	0.97
Koutas and Bournas (2017)	C1	0.095	974		14.29		207	172		0.83	
	C2	0.19	840		20.16		291	241		0.83	
	C1-part	0.0475	1,223		11.24		178	135		0.76	
	G3	0.132	300		9.47		142	114		0.80	

broken partly. Therefore, the results were more accurate when the Eqs. (16) to (27) was used to strengthened slab. According to Table 8, it could be seen that the theoretical values were all smaller than the experimental values, and the structure had a certain safety reserve that meets the reliability requirements. When using method in this paper to calculate the square TRM strengthened RC slab (Koutas and Bournas, 2017), the average ratio of the theoretical value to the experimental value was 0.81, which was in good agreement and safe enough. And it was suitable for RC slab strengthened with different types and different layers of fiber net.

In this paper, the effective stress actually exerted by CFN when the slab failed were 1,081 MPa and 1,388 MPa in the x and y directions respectively. In the square slab tested by Koutas, the effective stress of the fiber net in the two directions were roughly equal. The data in Table 5 showed that when the textile ratio increased from 0.0475% to 0.19%, the effective stress value of the fiber net decreased from 1,223 MPa to 840 MPa, that is, the higher the textile ratio, the lower the effective stress value of the fiber net. Therefore, when TRM was used for flexural strengthening of structural members, the actual stress exerted by the fiber net in FRPM was reduced from the stress when it was subjected to load alone. This factor should be considered when using TRM for strengthening in actual projects.

6. Conclusions

This paper performed experimental investigation on 3 RC two-way slabs strengthened with TRM, mainly studied the influence of different interface treatment on flexural strengthening. In addition, a calculation model was proposed using the method of plastic hinge line based on the results. The main conclusions were drew in a concisely manner as follows:

1. Compared with the unstrengthened slab, the ultimate load, the pre-cracking stiffness, the post-cracking stiffness and energy absorption values of RC two-way slabs unstrengthened with CFN reinforced mortar increased by 43.8%, 24.2%, 83.4%, and 49.1%, respectively. This indicated that CFN reinforced mortar reinforcement could significantly improve the bearing capacity, stiffness and energy consumption capacity of RC two-way slabs.
2. Compared with the unstrengthened slab, the ultimate load, the pre-cracking stiffness, the post-cracking stiffness and energy absorption values of the RC two-way slabs unstrengthened with CFN reinforced mortar treated with epoxy interface agent increased by 54.2%, 47.8%, 145.2%, and 75.5%, respectively. The application of epoxy based interface agent can significantly improve the bearing capacity, stiffness, and energy absorption value of RC two-way slabs, and can suppress local debonding between TRM reinforcement layer and the RC slab, preventing crack propagation along the interface direction.
3. The theoretical bearing capacity of TRM strengthened the two-way RC slab under different plastic hinge modes was different. Under plastic hinge mode II in this paper, the theoretical bearing capacity was in good agreement with the experimental value.
4. This paper proposed the concept of strength utilization rate and found that there was a functional relationship between it and the textile ratio, which was in good agreement with the experimental value.

But due to the limitation of the experimental data, the reduction factor under different textile ratios and specimen sizes needs more experiments and theoretical studies to prove it. Based on the seismic shear capacity formula of masonry wall with constructional column, the formula for design shear capacity of the wall strengthened with fiber nets is deduced. In the future, further research will be conducted on the bending performance of two-way slabs strengthened with different types of nets, layers, reinforced polymer mortar or ultra-high performance concrete.

Acknowledgments

Not Applicable

ORCID

Not Applicable

References

Al-Salloum YA, Siddiqui NA, Elsanadedy HM, Abadel AA, Aqel MA (2011) Textile-reinforced mortar versus FRP as strengthening material for seismically deficient RC beam-column joints. *Journal of Composites for Construction* 15:920-933, DOI: 10.1061/(ASCE)CC.1943-5614. 0000222

Azam R, Soudki K (2014) FRCM strengthening of shear-critical RC beams. *Journal of Composites for Construction* 18:04014012, DOI: 10.1061/(ASCE)CC.1943-5614.0000464

Babaeidarabad S, Loreto G, Nanni A (2014) Flexural strengthening of RC beams with an externally bonded fabric-reinforced cementitious matrix. *Journal of Composites for Construction* 18:3049-3060, DOI: 10.1061/(ASCE)CC.1943-5614.0000473

Bournas DA,Lontou PV,Papanicolaou CG, Triantafillou TC (2007) Textile-reinforced mortar versus fiber-reinforced polymer confinement in reinforced concrete columns. *ACI Structural Journal* 104:740-748, DOI: 10.14359/18956

Burgess I (2017) Yield-line plasticity and tensile membrane action in lightly-reinforced rectangular concrete slabs. *Engineering Structures* 138:195-214, DOI: 10.1016/j.engstruct.2017.01.072

D'Ambrisi A, Feo L, Focacci F (2012) Bond-slip relations for PBO-FRCM materials externally bonded to concrete. *Composite Part B: Engineering* 43:2938-2949, DOI: 10.1016/j.compositesb.2012.06.002

D'Ambrisi A, Focacci F (2011) Flexural strengthening of RC beams with cement-based composites. *Journal of Composites for Construction* 15:707-720, DOI: 10.1061/(ASCE)CC.1943-5614.0000218

Deng ZC, Gong MG (2022) Experimental study on biaxial flexural behaviors of textile reinforced concrete slab with hybrid Fibers. *Journal of Beijing University of Technology* 48(4):367-377, DOI: 10.11936/bjutxb2020110042

Deng ZC, Lu YH, Gui YJ (2022) Flexural properties of ultra-high performance concrete reinforced with steel wire mesh or fiber mesh.

Acta Materiae Compositae Sinica 39(10):4757-4768, DOI: 10.13801/j.cnki.fhclxb.20211022.002

Ebead U (2015) Inexpensive strengthening technique for partially loaded reinforced concrete beams: Experimental study. *Journal of Materials in Civil Engineering* 27:04015002, DOI: 10.1061/(ASCE)MT.1943-5533.0001249

Ebead U, Shrestha KC, Ahmed MS Refai El, Nanni A (2016) Effectiveness of fabric-reinforced cementitious matrix in strengthening reinforced concrete beams. *Journal of Composites for Construction* 21: 04016084, DOI: 10.1061/(ASCE)CC.1943-5614.0000741

Koutas LN, Bournas DA (2017) Flexural strengthening of two-way RC slabs with textile-reinforced mortar: Experimental investigation and design equations. *Journal of Composites for Construction* 21: 04016065, DOI: 10.1061/(ASCE)CC.1943-5614.0000713

Koutas LN, Zoi Tetta, Bournas DA, Triantafillou TC (2019) Strengthening of concrete structures with textile reinforced mortars: State-of-the-art review. *Doctoral dissertation, American Society of Civil Engineers* 27:958-961, DOI: 10.1061/(ASCE)CC.1943-5614.0000882

Loreto G, Leardini L, Arboleda D, Nanni A (2013) Performance of RC slab-type elements strengthened with fabric-reinforced cementitious-matrix composites. *Journal of Composites for Construction* 18:213-226, DOI: 10.1061/(ASCE)CC.1943-5614.0000415

Ombres L (2012) Flexural analysis of reinforced concrete beams strengthened with a cement based high strength composite material. *Composites Structures* 94:143-155, DOI: 10.1016/j.compstruct.2011.07.008

Papanicolaou C, Triantafillou T, Papantoniou I, Balioukos C (2009) Strengthening of two-way reinforced concrete slabs with Textile Reinforced Mortars (TRM). 4th Colloquium on Textile Reinforced Structures (CTRS4), Dresden, Germany 409-420

Rüsch H (1960) Researches toward a general flexural theory for structural concrete. *Journal of the American Concrete Institute* 57:1-28, DOI: 10.14359/8009

Scheerer S, Schladitz F, Curbach M (2015) Textile reinforced concrete–from the idea to a high performance material. Proceedings of the FERRO-11—11th International Symposium on Ferrocement and 3rd ICTRC–International Conference on Textile Reinforced Concrete, Aachen, Germany 7-10

Scheerer S, Zobel R, Egbert Müller, Senckpiel-Peters T, Schmidt A, Curbach M (2019) Flexural strengthening of RC structures with TRC–Experimental observations, design approach and plication. *Applied Sciences* 9:1322, DOI: 10.3390/app9071322

Schladitz F, Frenzel M ,Ehlig D, Curbach M (2012) Bending load capacity of reinforced concrete slabs strengthened with textile reinforced concrete. *Engineering Structures* 40:317-326, DOI: 10.1016/j.engstruct.2012.02.029

Sneed LH Verre S, Carloni C, Ombres L (2016) Flexural behaviour of RC beams strengthened with steel-FRCM composite. *Engineering Structures* 127: 686-699, DOI: 10.1016/j.engstruct.2016.09.006

Thermou GE, Katakalos K, Manos G (2015) Concrete confinement with steel-reinforced grout jackets. *Materials and Structures* 48:1355-1376, DOI: 10.1617/s11527-013-0239-6

Trapko T, Urbańska D, Kamiński M (2015) Shear strengthening of reinforced concrete beams with PBO-FRCM composites. *Composites Part B Engineering* 80:63-72, DOI: 10.1016/j.compositesb.2015.05.024

Triantafillou TC, Papanicolaou CG (2006) Shear strengthening of reinforced concrete members with textile reinforced mortar (TRM) jackets. *Materials and Structures* 391:93-103, DOI: 10.1617/s11527-005-9034-3

Yin SP, Peng C, Jin ZY (2017) Research on mechanical properties of axial-compressive concrete columns strengthened with TRC under a conventional and chloride wet-dry cycle environment. *Journal of Composites for Construction* 21:04016061, DOI: 10.1061/(ASCE)CC.1943-5614.0000725